1   **A fluorinated phenylbenzothiazole arrest the *Trypanosoma cruzi* cell cycle and**

2   **diminishes the mammalian host-cell infection**

3   Roberto I. Cuevas-Hernández[a,b], Richard M.B.M. Girard[b], Sarai Martínez-Cerón[a],

4   Marcelo Santos da Silva[c,d], Maria Carolina Elias[c,d], Marcell Crispim[b], José G. Trujillo-

5   Ferrara[a#] and Ariel Mariano Silber[b#].

6

7   [a]Laboratory of Biochemistry Research, Escuela Superior de Medicina, Instituto

8   Politécnico Nacional, México. Plan de San Luis Y Díaz Mirón S/N, Casco de Santo

9   Tomas, Miguel Hidalgo, ZIP: 11340 Mexico City, Mexico.

10   [b]Laboratory of Biochemistry of Tryps - LaBTryps, Department of Parasitology, Institute

11   of Biomedical Sciences, University of São Paulo. Av. Lineu Prestes 1374, Cidade

12   Universitária CEP: 05508-000, Butantã, São Paulo - SP - Brazil.

13   [c]Special Laboratory of Cell Cycle, Butantan Institute, Av. Vital Brasil 1500 (05503-

14   900), São Paulo - SP – BRAZIL.

15   [d]Centre of Toxins, Immune Response and Cell Signalling – CeTICS, Butantan Institute,

16   Av. Vital Brasil 1500 (05503-900), São Paulo - SP - BRAZIL.

17

18   # Both are corresponding authors together:

19   Ariel Mariano Silber (AMS) Tel.: +55-11-3091-7335; e-mail: asilber@usp.br

20   José G. Trujillo-Ferrara (JGTF) Tel.: +52 1 55-5729-6000 ext. 62747; e-mail:

21   jtrujillo@ipn.mx

22

23   **Running title:** BT10 triggers cell cycle arrest in *T. cruzi*

24

25 **Keywords:** Phenylbenzothiazole, Chemotherapy, *Trypanosoma cruzi*, kDNA,

26 Antiparasitic agents

27

28 **Abstract**

29 Chagas disease (CD) is a human infection caused by *Trypanosoma cruzi*. CD was

30 traditionally endemic to the Americas, however, due to migration it has spread to non-

31 endemic countries. The current chemotherapy to treat CD induce several side effects

32 and its effectiveness in the chronic phase of the disease is controversial. In this

33 contribution, substituted phenylbenzothiazole derivatives were synthesized and

34 biologically evaluated as trypanocidal agents against *Trypanosoma cruzi*. The

35 trypanocidal activities of the most promising compounds were determined through

36 systematic *in vitro* screening and their mode of action as well. The physicochemical-

37 structural characteristics responsible for the trypanocidal effects were identified, and

38 their possible therapeutic application in Chagas disease is discussed. Our results show

39 that the fluorinated compound, 2-methoxy-4-[5-(trifluoromethyl)-1,3-benzothiazol-2-yl]

40 phenol (BT10) has the ability to inhibit the proliferation of epimastigotes ($IC_{50(Epi)}$ =

41 23.1 ± 1.75 μM) and intracellular forms trypomastigote ($IC_{50(Tryp)}$ = 8.5 ± 2.9 μM) and

42 diminishes the infection index by more than 80%. In addition, BT10 has the ability to

43 selectively fragment 68% of the kinetoplastid DNA compared with 5% of nucleus

44 DNA. The mode of action for BT10 on *T. cruzi* suggests that the development of

45 fluorinated phenylbenzothiazole with electron-withdrawing substituent could be a

46 promising strategy for the design of trypanocidal drugs.

47

48

49

50 **Introduction**

51 American trypanosomiasis or Chagas disease (CD) is a zoonosis caused by the

52 flagellated intracellular protist *Trypanosoma cruzi*. According to the World Health

53 Organization (WHO), CD is endemic in the Americas; however, due to migration, it has

54 spread to non-endemic countries such as Canada and several European and Western

55 Pacific countries (1, 2). This disease, with approximately 7 million affected people,

56 causes approximately 14 thousand deaths annually, and there are 70 million at risk of

57 becoming infected (3). *T. cruzi,* which is naturally transmitted by hematophagous

58 insects of the *Reduviidae* family, can also be transmitted by other routes, such as

59 congenitally (from an infected pregnant woman to the foetus), orally (through

60 contaminated foods and liquids), and through organ transplantations and blood

61 transfusions (4).

62 *T. cruzi* has a complex life cycle, which occurs within invertebrate and vertebrate hosts

63 (5–7). Replicative, non-infective epimastigotes present in the insect vector give rise to

64 non-replicative infective metacyclic trypomastigotes. These forms invade the host cell,

65 establish the infection and differentiate into replicative amastigotes. Amastigote forms

66 give rise to a transient stage named intracellular epimastigotes, which subsequently

67 differentiate into trypomastigotes that can disseminate in the mammalian host through

68 the bloodstream after causing lysis of host cells and are capable of infecting other cells.

69 The insect vector can acquire these forms during its bloodmeal, becoming infected and

70 able to infect a new mammalian host (8, 9).

71 Human infection is characterized by two sequential clinical phases: acute and chronic.

72 The acute phase is often asymptomatic and usually remains undiagnosed. Most infected

73 individuals proceed to the chronic phase, which lasts for the rest of the patient´s life.

74 The chronic phase presents several clinical forms: 70% of patients are asymptomatic,

3

75   while the remaining 30% present clinical manifestations, with the most frequent being

76   chagasic chronic cardiomyopathy and, more rarely, megavisceras (mainly megacolon

77   and megaoesophagus). Over years, the cardiac form of the infection can cause sudden

78   death or heart failure due to the progressive destruction of the cardiac muscle (9).

79   A century after the discovery of the disease by Carlos Chagas in 1909, only two

80   nitroheterocyclic drugs, nifurtimox, and benznidazole, are used to treat *T. cruzi*

81   infection. These drugs are effective during acute infection. However, their effectiveness

82   during the chronic phase of CD is controversial due to their toxicity (10). Therefore,

83   more secure, effective and accessible alternatives are currently being sought to treat CD.

84   *T. cruzi,* along with other trypanosomatids, possesses unique morphological and

85   metabolic features, offering opportunities for looking for selective inhibitors. Among

86   them, it is worth mentioning the kinetoplast, a complex structure bearing the

87   mitochondrial genome referred to as kinetoplast DNA or kDNA. The kDNA consists of

88   a large number of relaxed circular DNA molecules interlocked with each other to form a

89   catenated DNA network, and this feature is among those that have frequently been

90   considered promising therapeutic targets because they are exclusive to trypanosomatids

91   (11).

92   In the last two decades, large libraries of compounds of diverse chemical nature have

93   been screened for trypanocidal agents (12). Among the selected chemical structures,

94   benzothiazoles (BZTs) have been studied in detail and have been suggested as

95   trypanocides (13–15). BZTs are a class of bicyclic compounds with a broad spectrum of

96   biological applications, such as neuroprotectors (16), anticonvulsants (17), antioxidants

97   (18), kinase inhibitors (19), anticancer agents (20, 21), antimicrobials (22) and

98   leishmanicidal (23). In particular, it has been suggested that the trypanocidal effects of

99   benzothiazoles are related to the inhibition of triosephosphate isomerase (TIM) (24, 25).

4

100   In previous work, we reported the development of 4-[5-(trifluoromethyl)-1,3-

101   benzothiazol-2-yl] benzoic acid, named BT3, which showed excellent trypanocidal

102   activity on bloodstream trypomastigotes of *T. cruzi* (14); thus, it was proposed as a new

103   nucleus for the development of trypanocidal agents. The aim of this contribution was to

104   determine the trypanocidal activity of a collection of 14 benzothiazoles structurally

105   related to BT3. We evaluated their anti-*T. cruzi* activity and we analyse their

106   physicochemical-structural characteristics responsible for its biological activity. BT10,

107   the most promising molecule due to its higher selectivity index than the other

108   derivatives, was selected for further analysing its effects on different aspects of *T. cruzi*

109   biology. We propose BT10 as a promising pharmacological hit compound for

110   developing a treatment against CD.

111

112   **RESULTS**

113   **BT10 affects the proliferation of *T. cruzi* epimastigotes**

114   A collection of 14 structurally related molecules, named BT1 to BT14 was synthesized

115   (**Figure 1A**). The identification of the synthesized molecules and their chemical

116   characterization were performed by melting point (mp), nuclear magnetic resonance

117   (NMR) and electrospray ionization – mass spectrometry spectra determination (ESI–

118   MS). These compounds were initially evaluated for their ability to inhibit epimastigote

119   proliferation in the presence of 25 μM BT1-14. We attributed a positive inhibition

120   activity to those compounds that, at the concentration used, were able to diminish the

121   cell density at the mid-exponential growth phase (which was measured on the 5th day

122   from the beginning of incubation) by 50% or more. Epimastigotes cultured in the

123   absence of drugs in the presence or absence of DMSO (which did not show significant

124   differences) were used as negative controls for inhibition, and their cell density was

125   considered as 100% proliferation. For a positive control for the inhibition of cell

5

126   proliferation, the parasites were incubated in the presence of a combination of 60 μM

127   rotenone + 0.5 μM antimycin (RA). The compound BT10 was identified as having

128   trypanocidal or trypanostatic activity. BT10 produced a diminution of cell density of

129   50% when compared to that of control (untreated) cultures. Despite not reaching the

130   criterion for selecting them as trypanocidal/trypanostatic, it is worth mentioning that

131   compounds BT3, BT9, and BT11 showed a modest but statistically significant decrease

132   in the cell density concentration when compared to that of controls (**Figure 1B and**

133   **Figure S1**). Because BT3 was used as lead (14) for choosing and synthesizing BT1-14,

134   it was selected for further experiments to use this information to unveil the

135   structure/activity relationship of these compounds.

136

137   To further evaluate the potency of BT3 and BT10 as anti-*T. cruzi* agents, we initially

138   determined their IC_{50} on epimastigote proliferation through dose-response experiments.

139   Cells were cultured in liver infusion tryptose (LIT) in the presence of different

140   concentrations of BT3 and BT10. As previously described, epimastigotes cultured in the

141   absence of drugs were used as negative controls for inhibition, and their cell density was

142   considered as 100% proliferation; parasites treated with RA were used as positive

143   controls for the inhibition of cell proliferation. As expected, BT3 and BT10 showed a

144   dose-dependent inhibition of epimastigote proliferation with IC_{50} values of 48.8 ± 5.77

145   μM and 23.1 ± 1.75 μM, respectively (**Figure 2A**, **2B**).

146

147   **BT10 does not induce programmed cell death (PCD)**

148   To characterize the mechanism of action of BT10, we initially investigated its ability to

149   trigger programmed cell death (PCD) in *T. cruzi* epimastigotes. For this analysis, we

150   investigated the typical PCD morphological, cellular and biochemical hallmarks in

6

151 trypanosomatids, such as ROS production, as well as Ca^{2+} and $\Delta\Psi_m$ imbalance (26, 27).

152 We initially looked for exposure of phosphatidylserine in the external leaflet of the

153 plasma membrane. Parasites were treated with 25 μM and 50 μM BT10 (approximately

154 1x and 2x the IC_{50}). After washing, they were incubated with Annexin V-FITC to assess

155 external exposure of phosphatidylserine and propidium iodide to assess plasma

156 membrane permeabilization. The cells were then subjected to analysis by flow

157 cytometry. The results showed that BT10 did not induce alterations in the plasma

158 membrane; no exposure of phosphatidylserine or signs of membrane permeabilization

159 were evidenced at both concentrations used in the assay when compared with that of the

160 controls (**Figure 3A, 3B, 3C**). We also investigated whether BT10 triggered other PCD

161 hallmarks, such as the dissipation of the mitochondrial inner membrane potential ($\Delta\Psi_m$),

162 production of reactive oxygen species (ROS), and changes in the cytosolic Ca^{2+} levels

163 (28). To analyse membrane depolarization ($\Delta\Psi_m$), parasites treated with 25 or 50 μM

164 BT10 (or not, control) during five days were stained with Rh123 for 20 min at 28 ºC

165 and further analysed by flow cytometry. Treated parasites showed a shift in the obtained

166 fluorescence values, showing an alteration of $\Delta\Psi_m$ (**Figure 3D**). To determine the

167 possible variations of the intracellular Ca^{2+} concentrations, epimastigotes were

168 incubated with 25 μM BT10 (or not, control) for five days. After treatment, the parasites

169 were incubated with Fluo-4 and analysed by flow cytometry. The results showed that

170 treated parasites exhibited increased intracellular Ca^{2+} concentrations compared with

171 those of untreated parasites (control) (**Figure 3E**). Finally, to evaluate possible changes

172 in the production of H_2O_2 due to treatment with BT10, epimastigotes treated with 25

173 μM BT10 for 24 hours (or not, control) were labelled with carboxy-DCFDA. The

174 results showed that the treated parasites did not produce a greater amount of H_2O_2 than

175 untreated parasites (**Figure 3F**). Taken together, these results indicate that BT10 does

176   not trigger any of the types of classic cell death as a primary effect, even at high

177   concentrations. However, mitochondrial inner membrane depolarization and alterations

178   in Ca^{2+} concentrations could be critical factors affecting the proliferation or long-term

179   survival of parasites.

180

181   As the previous results suggest that BT10 did not trigger cell death, we hypothesized

182   that the drug interferes with the *T. cruzi* cell cycle. To confirm this possibility, we

183   evaluated the reversibility of the effect of BT10 on epimastigote proliferation.

184   Epimastigotes were treated or not (control) with 25 μM and 100 μM BT10. The treated

185   parasites showed diminished proliferation during the treatment with respect to that of

186   the controls. This alteration was reversed by washing out BT10, indicating that BT10

187   reversibly inhibited epimastigote proliferation (**Figure S2**). On this basis, we further

188   analysed possible alterations in the cell cycle. Parasites treated with 25 μM and 100 μM

189   BT10 or left untreated (control) for five days were labelled with propidium iodide and

190   submitted to cell cycle analysis by flow cytometry (**Figure 4A**). The data collected

191   showed a significant decrease in cells in the G_0/G_1 phases and an accumulation in the

192   G_2/M phase with significant alterations in the S phase at 100 μM BT10 compared to

193   those in the control cells (**Figure 4B**).

194

195   Importantly, an accumulation of cells in the G2/M phases is usually due to an arrest of

196   the cell cycle at G_2 checkpoint, in which DNA integrity is sensed and checked (29).

197   Because cell cycle arrest can be induced at G_2 checkpoint by DNA damage (30, 31), we

198   investigated whether BT10 causes DNA damage to treated parasites. We analysed the

199   effect of BT10 on both genomic DNA (gDNA) and kDNA integrity using a TUNEL

200   assay. Epimastigotes treated for 5 days with 25 μM BT10 (or left untreated as a control)

8

201   were submitted to the TUNEL assay. The parasites were initially analysed by flow

202   cytometry, showing differences in fluorescence intensity in the treated population with

203   respect to that of the control (**Figure 5B**). When the parasites were analysed by

204   microscopy, we found that the kDNA was intensively labelled when compared to the

205   gDNA in the parasites treated with BT10. Untreated parasites and treated parasites

206   exhibited 35.2 ± 6.2 % and 67.6 ± 8.6 % of cells with labelled kDNA, respectively. On

207   the other hand, the percentage of treated parasited with labelled gDNA was 5.4 ± 1.2%

208   while the untreated parasites remain unlabelled. These data indicate that BT10

209   selectively triggers kDNA damage (**Figure 5A**). Taken together, these data indicate that

210   BT10 induces DNA double-strand breaks preferentially on kDNA.

211

212   **Cytotoxicity of BT3 and BT10 to mammalian cells**

213   To further evaluate the effect of BT10 on the stages corresponding to mammalian host

214   cell infection, it is necessary first to determine the range in which the compounds are

215   non-toxic for the host cells. Therefore, CHO-K_1 cells were incubated in the presence of

216   different concentrations of BT3 (ranging from 16 to 800 μM) or BT10 (ranging from 8

217   to 288 μM), and cytotoxicity was evaluated by MTT assay after 48 h of treatment. The

218   concentrations corresponding to a measurement of 50% cytotoxicity (CC_{50}) were

219   obtained from the typical sigmoidal concentration-response curves, resulting in 95.3 ±

220   3.3 μM for BT10 and 127.6 ± 0.9 μM for BT3 (**Figures 6A, 6B**).

221

222   **BT10 selectively inhibits the intracellular cycle of *T. cruzi***

223   According to the results obtained from the cytotoxicity experiments, a range of BT10

224   concentrations from 0.1 to 32 μM was selected to evaluate the IC_{50} for trypomastigote

225   release after an entire infection cycle on CHO-K_1 cells. To measure the effect of BT10

9

226   on trypomastigote production by infected host cells, CHO-K$_1$ cells were incubated with

227   trypomastigotes for 4 h. The cells were washed to eliminate the non-internalized

228   parasites and then incubated with culture medium at different concentrations of BT10 or

229   not (control). On the 5th day post-infection, the trypomastigotes released into the culture

230   media were counted. We observed a dose-dependent decrease in trypomastigote release,

231   which allowed us to measure the IC$_{50}$ for trypomastigote bursting (8.5 ± 2.9 μM)

232   (**Figure 7A, 7B**). Based on this value and the CC$_{50}$ obtained for the cytotoxicity of

233   BT10 on CHO-K$_1$ cells, we obtained a selectivity index (SI; CC$_{50}$/IC$_{50(Tryp)}$) of 11.21. It

234   is expected that the diminished number of burst trypomastigotes in the BT10-treated

235   cells is a reflection of the diminished proliferation of intracellular forms. To verify this

236   hypothesis, CHO-K$_1$ cells were incubated with trypomastigotes for 4 h. The cells were

237   washed to eliminate the non-internalized parasites, and then they were incubated with

238   culture medium supplemented or not (control) with 8.5 μM BT10 (the concentration

239   corresponding to the IC$_{50}$ obtained for trypomastigote bursting). On the second day

240   post-infection, the cultures were fixed and stained, and the nuclei corresponding to the

241   total number of cells, the number of infected cells, and the number of amastigotes per

242   infected cell were counted. The percentage of infected cells and the number of

243   intracellular amastigotes per cell were 8.6 ± 0.88 and 0.16 ± 0.05 for infected cells

244   treated with 8.5 μM of BT10 and 13.1 ± 3.7 and 0.6 ± 0.13 for untreated conditions,

245   respectively **(Figure 7C, 7D)**. BT10 treatment diminished the number of infected cells

246   by 33.8% and the average number of intracellular amastigotes per cell by 70.3%. The

247   resulting infection index was 1.4 ± 0.48 for the treated infected cells and 8.9 ± 1.34 for

248   the controls, indicating that the treatment reduced the infection index by 81.3 ± 6.94 %

249   (**Figure 7E, 7F**). Taken together, these results indicate that treatment with 8.5 μM BT10

250   interferes with proliferation and/or differentiation of intracellular stages (**Figure 7**).

10

251

252

253

DISCUSSION

In the present work, we obtained and evaluated a collection of 14 benzothiazoles (BT1-

14) related to previously studied 4-[5-(trifluoromethyl)-1,3-benzothiazol-2-yl] benzoic

acid (BT3), which showed relevant anti-*T. cruzi* trypomastigote activity (14). The anti-

proliferation activity for all these compounds was initially evaluated in a screening with

25 μM each compound. BT10 was the only one that diminish the epimastigote growth

by 50%, as previously mentioned. Although BT3 did not pass these criteria, it was the

second best in terms of potency. Thus, BT10 and BT3 were used for some experiments

that allowed us to infer some structure-activity relationships. Both compounds contain a

trifluoromethyl group (-CF$_3$) in the R^1 position of the benzothiazole moiety.

Additionally, BT3 has a carboxyl group (-COOH) on R^3 of the phenyl moiety, while

BT10 contains a methoxy group (-OCH$_3$) on R^2 and a hydroxyl group (-OH) on R^3.

These data suggest that the inclusion of a fluorinated group on 2-phenylbenzothiazole

derivatives contributes significantly to the anti-proliferation activity. All these

inferences are supported by the fact that benzothiazole derivatives such as (*S*)-2-(3,4-

difluorophenyl)-5-(3-fluoro-*N*-pyrrolidylamido) benzothiazole possess anti-

Trypanosoma brucei activities (15). BT2 and BT6 compounds are closely related to

BT3 and BT10, respectively, with the only difference being the absence of the -CF$_3$

substituent. The relevance of the fluorinated group in BT2 and BT6 could explain their

lack of anti-*T. cruzi* activity (**Figure 1A, 1B, 1C**). In fact, this finding is not surprising

since it is well known that fluorine atoms confer a set of physicochemical properties to

organic compounds. Among them, it is worth mentioning improvement of lipophilicity,

11

276   increased velocity of diffusion through biological membranes (32), an improved affinity

277   for receptors (by favouring electrostatic interactions) and an increased binding affinity

278   to active sites (33). In addition, the presence of fluorinated groups can also modify the

279   acidity or basicity of the molecules, affecting the processes of absorption, metabolism

280   and bioavailability (34). To analyse the correlation of the activity of BT1-14 to *in silico*

281   drug-likeness analysis (rule of five – RO5) (35), we determined whether the compounds

282   in the collection follow these rules. Regarding the quantitative parameters of the RO5,

283   we calculated the lipophilicity (expressed as the partition coefficient - Log P) and

284   topological polar surface area (TPSA - defined as the integration of the surfaces of polar

285   atoms (in this case oxygen, nitrogen, and attached hydrogen) (36). The computed

286   parameters showed that BT3 and BT10 have Log P values of 3.83 and 3.92 and TPSA

287   values of 78.43 and 70.59, respectively. The presence of the $-CF_3$ group affected the

288   predicted lipophilicity (comparing BT2 with BT3 and BT6 with BT10), resulting in

289   intermediate Log P values for the most active compounds. However, BT3 and BT10

290   were among those presenting the highest TPSA values in the collection. The increased

291   TPSA values are probably due to the -COOH, -OH and $-OCH_3$ groups on the phenyl

292   moiety, which trigger electron withdrawal in combination with the –CF3 group in the

293   case of BT10 and BT3. This fact could have a positive effect on anti-proliferation

294   activity. As the drug-likeness depends on both values, we propose herein a parameter

295   consisting of the product between Log P and TPSA **(Table S1),** which showed for our

296   compounds a good prediction capacity in relation to their *in vitro* activity.

297   Among the drugs analysed in our collection, BT10 was the only one that passed through

298   our criteria for being selected as an anti-*T. cruzi* drug for further studies, resulting in 2-

299   fold more potent activity than that of BT3. Despite its anti-proliferation effect, we could

300   not detect signals of cell death in BT10-treated parasites, such as exposure of

12

301   phosphatidylserine or loss of cytoplasmic membrane integrity. Thus, we hypothesized

302   that BT10 would act as a trypanostatic compound rather than a trypanocide. Despite

303   having a lower activity, we observed the same profile for BT3-treated parasites

304   (**Figure S3**), indicating that the mode of action of these structurally related

305   compounds in *T. cruzi* is other than cytotoxicity, as previously reported for other

306   benzothiazoles when evaluated on different cancer cell lines (37, 38). To obtain more

307   clues about the inhibitory activity of BT10, we explored other parameters related to the

308   maintenance of cell viability: the status of the mitochondrial inner membrane potential

309   ($\Delta\Psi m$), intracellular Ca^{2+} levels and endogenous production of ROS (26, 28). Our

310   results show that a fraction of the BT10-treated cells had a diminished $\Delta\Psi m$ with

311   respect to that of the controls. This result indicates that their mitochondria are at least

312   partially depolarized, which is consistent with the observed increase in intracellular Ca^{2+}

313   concentration.

314   Altogether, our results agree in part with the effects reported for benzothiazoles with

315   antimicrobial activity in both Gram-positive and Gram-negative bacteria, although the

316   effects are observed with 4-fold the minimum inhibitory concentration (between 3.91 -

317   15.6 μg / mL) (39). Notably, these effects by themselves point to a trypanostatic rather

318   than trypanocidal activity. This possibility was confirmed by the fact that the effect of

319   BT10 was reversible and produced alterations in the epimastigote cell cycle. Indeed,

320   BT10 triggered a decrease of parasites in G_0/G_1 phases and an accumulation in the G/M

321   phase at a concentration of 100 μM.

322   An alteration of the cell cycle consisting of the accumulation of parasites in the G/M

323   phase could be a hallmark for DNA damage (31, 40). Our results revealed that BT10-

324   and BT3-treated cells (**Figure S4**) had selectively damaged kDNA, raising three

325   possibilities: i. kDNA has a higher sensitivity to damage than gDNA; ii. the

13

326   mitochondrial DNA repair machinery (in the presence of the drug) is less efficient than

327   that of the nuclear DNA; or iii. the drug accumulates at higher concentrations in the

328   mitochondria, submitting kDNA to higher concentrations of the drug than those for

329   gDNA. Of course, a combination of the three possibilities cannot be ruled out. In any

330   case, the mechanism by which damage occurs to kDNA remains elusive; it is possible

331   that BT10 and BT3 will inhibit some DNA-dependent enzyme or inhibitor directly by

332   inhibition of transcription and replication enzymes through direct interaction with DNA,

333   as suggested by the helically arranged relationship of BT6 in crystal formation (41).

334   This work support the fact that the kDNA seems to be the main target to explain the

335   anti-*T. cruzi* effect of BT3 and BT10. Indeed, the concentrations required to inhibit the

336   triosephosphate isomerase are higher than those required to kill trypanosomatids (14,

337   15, 23). These data break the paradigm that the trypanocidal effect of benzothiazoles is

338   due to the inhibition of triosephosphate isomerase as traditionally proposed (13, 25, 42).

339   Regardless of the mechanism of action, the anti-*T. cruzi* activity on the parasite stages

340   that are relevant for mammalian infection is a *sine qua non* condition for any compound

341   to be proposed as a possible drug to develop a treatment against Chagas disease.

342   Remarkably, the treatment of infected cells with 8.5 µM BT10 caused a significant

343   reduction in the number of intracellular amastigotes, in the trypomastigote burst and in

344   the infection index. These results, together with the drug selectivity (SI of 11.21) (**Table

345   1),** are particularly promising for the development of chemotherapy against the chronic

346   phase of the disease.

347   To conclude, BT10 is a remarkable fluorinated hit compound for the development of

348   new and better anti-*T. cruzi* compounds, which would be in accordance with the

349   initiative proposed by the Drugs for Neglected Diseases initiative (DNDi) (43). Because

350   the kinetoplast is the preferred target for BT10, other compounds based on its structure

14

351   could have potential therapeutic applications for other diseases caused by kinetoplastid

352   parasites, such as *Leishmania spp.* and *T. brucei*.

353

354   **Materials and methods**

355   **Reagents.** All chemicals, reagents, and solvents for synthesis and MTT

356   (methylthiazolyldiphenyl-tetrazolium bromide) were purchased from Sigma-Aldrich

357   (St. Louis, MO, USA); Fluo-4 AM and Annexin V-FITC were purchased from

358   Invitrogen (Eugene, Oregon, USA); and culture media and foetal calf serum (FCS) were

359   purchased from Cultilab (Campinas, SP, Brazil).

360

361   **Synthesis of drugs and chemical characterization.** The 2-phenylbenzothiazole

362   derivatives were synthesized by the following reaction conditions previously described

363   (14). Briefly, the appropriate 2-aminothiophenol (1.98 mmol) and substituted

364   benzaldehyde (2.1 mmol) were reacted with an equimolar amount of $Na_2S_2O_5$ (2.1

365   mmol). The mixture, was stirred refluxing in DMSO at ~120 °C for 40 - 60 min. The

366   product was precipitate by adding cool water and collected by vacuum filtration. The

367   filtrate was then washed with an excess of water and left to dry. The remaining traces of

368   sodium metabisulfite were extracted with brine and CH_2Cl_2, and the solvent was

369   removed under vacuum. Finally, the resulting product was purified and recrystallized in

370   ethanol/water (1:3). The progress of the reaction was monitored by TLC analysis using

371   a mix of ethyl acetate/hexane (1:1) as the eluent. All synthesized products were

372   chemically characterized by ^{1}H, ^{13}C NMR spectra on a Jeol GSX-300 spectrometer (^{1}H

373   300 MHz, ^{13}C 75 MHz) or Bruker-400 (^{1}H 400 MHz, ^{13}C 101 MHz) or Bruker-750

374   biospin Rheinstetten, Germany (^{1}H 750 MHz, ^{13}C 189 MHz) using DMSO-d_6 and

375   CDCl$_3$ as the solvent and TMS as the internal reference. Chemical shift values (δ_{ax}) are

376 presented in parts per million (ppm), and coupling constants (*J* values) are presented in

377 Hertz (Hz). ESI – MS spectra were recorded on a Bruker micrOTOF-Q II. The

378 uncorrected melting points were obtained in open-ended capillary tubes in

379 Electrothermal 9300 digital equipment.

380

381 **BT1** (2-phenyl-1,3-benzothiazole): white needles, 77 % yield. mp 95-96 ℃. ^{1}H NMR

382 (400 MHz, CDCl$_3$) δ 8.08 (m, 3H), 7.89 (dd, 1H, ^3J= *8 Hz,* ^4J= *0.8 Hz*), 7.5 (t, 1H,

383 *J=1.2 Hz*), 7.48 (m, 3H), 7.37 (td, 1H, ^3J= 1.2 Hz); ^{13}C NMR (101 MHz, CDCl$_3$) δ

384 168.0, 154.1, 135.1, 133.6, 130.9, 129.0 (2C), 127.5 (2C), 126.3, 125.1, 123.2, 121.6;

385 MS(ESI) C$_{13}$H$_9$NS, [M + H]$^+$, m/z calcd 212.0528, found 212.0520.

386

387 **BT2** (4-(1,3-benzothiazol-2-yl)benzoic acid): white powder, 63 % yield. mp 332 ℃. [1]H

388 NMR (400 MHz, DMSO-d$_6$) δ 8.20 (d, 2H, ^3J = 8.4 Hz), 8.17 (s, 1H), 8.12 (d, 3H, ^3J =

389 8.0 Hz), 7.58 (t, 1H, ^3J = 7.6 Hz), 7.50 (t, 1H, ^3J = 7.6 Hz); ^{13}C NMR (101 MHz,

390 DMSO-d$_6$) δ 167.1, 166.6, 154.0, 136.8, 135.2, 133.7, 130.7 (2C), 127.7 (2C), 127.3,

391 126.4, 123.6, 122.9; MS(ESI) C$_{14}$H$_9$NO$_2$S, [M + H]$^+$, m/z calcd 256.0426, found

392 256.0394.

393

394 **BT3** (4-[5-(trifluoromethyl)-1,3-benzothiazol-2-yl]benzoic acid): white needles, 82 %

395 yield. mp 257 ℃ ^{1}H NMR (300 MHz, DMSO-d$_6$) δ 13.2 (s, 1H), 8.36 (d, 1H, ^3J= 6.6

396 Hz), 8.15 (d, 2H, ^3J= 8.4 Hz), 8.06 (d, 2H, ^3J= 8.7 Hz), 7.73 (dd, 1H, ^3J= 8.7, ^4J= 1.5

397 Hz); ^{13}C NMR (75 MHz, DMSO-d$_6$) δ 169.2, 166.9, 153.4, 139.2, 136.1, 133.8, 130.7

398 (2C), 128.3, 127.9 (2), 124.4, 122.2, 120.3; MS(ESI) C$_{15}$H$_8$F$_3$NO$_2$S, [M + H]$^-$, m/z calcd

399 322.0144, found 322.0226.

400

16

401 **BT4** (2-phenyl-5-(trifluoromethyl)-1,3-benzothiazole): yellow scaly crystals, 53 %

402 yield. mp 127-129 ℃. [1]NMR (400 MHz, CDCl$_3$) δ 8.33 (t, 1H, J= 0.8 Hz), 8.09 (m,

403 2H), 8.0 (dt, 1H, ^3J= 8.6 Hz, ^4J= 0.4 Hz), 7.52 (m, 3H); ^{13}C NMR (101 MHz, CDCl$_3$) δ

404 170.1, 153.7, 138.4, 133.0, 131.5, 129.1 (2C), 127.7 (2C), 125.5, 122.2, 121.5, 120.4;

405 MS(ESI) C$_{14}$H$_8$F$_3$NS, [M + H]$^+$, m/z calcd 280.0402, found 280.0379.

406

407 **BT5** (methyl 4-[5-(trifluoromethyl)-1,3-benzothiazol-2-yl]-benzoate): white needles,

408 41 % yield. mp 242 ℃. ^{1}H NMR (300 MHz, DMSO-d$_6$) δ 8.43 (s, 1H), 8.41 (s, 1H),

409 8.21 (d, 2H, ^3J= 11.2 Hz), 8.09 (d, 2H, ^3J= 11.2 Hz), 7.78 (d, 1H, ^3J= 11.2 Hz), 3.87 (s,

410 3H); ^{13}C NMR (75 MHz, DMSO-d$_6$) δ 169.1, 165.9, 153.6, 139.3, 136.7, 132.8, 130.5

411 (2C), 128.6, 128.1 (2C), 124.3, 122.3, 120.4, 52.7; MS(ESI) C$_{16}$H$_{10}$F$_3$NO$_2$S, [M + H]$^+$,

412 m/z calcd 338.0457, found 338.0452.

413

414 **BT6** (2-(4-hydroxy-3-methoxyphenyl)-benzothiazole): grey powder, 87 % yield. mp

415 162-163 ℃. ^{1}H NMR (300 MHz, DMSO-d$_6$) δ 9.85 (s, 1H), 8.03 (d, 1H, ^3J=8.25 Hz),

416 7.97 (d, 1H, ^3J= 8.4 ppm), 7.61 (d, 1H, ^4J= 2.1 Hz), 7.47 (dd, 1H, ^3J= 8.1 Hz, ^4J= 2.1

417 Hz), 7.47 (m, 1H), 7.37 (td, 1H, J= 7.6 Hz), 6.91 (d, 1H, J= 8.1 Hz), 3.87 (s, 3H); ^{13}C

418 NMR (75 MHz, DMSO-d$_6$) δ 167.9, 154.0, 150.4, 148.5, 134.6, 126.8, 125.3, 124.7,

419 122.7, 122.5, 121.7, 116.3, 110.4, 56.1; MS(ESI) C$_{14}$H$_{11}$NO$_2$S, [M + H]$^+$, m/z calcd

420 258.0583, found 258.0583.

421

422 **BT7** (3-(1,3-benzothiazol-2-yl)-benzoic acid): grey crystals, 77 % yield. mp 257 ℃. ^{1}H

423 NMR (750 MHz, DMSO-d$_6$) δ 13.40 (s, 1H), 8.63 (s, 1H), 8.31 (d, 1H, ^3J= 4.4 Hz),

424 8.18 (d, 1H, ^3J= 4 Hz), 8.12 (d, 1H, ^3J= 4.4 Hz), 8.1 (d, 1H, ^3J= 4.4 Hz), 7.72 (t, 1H,

425 ^3J= 4), 7.57 (t, 1H, ^3J= 4), 7.49 (t, 1H, ^3J= 3.8 Hz); ^{13}C NMR (189 MHz, DMSO-d$_6$) δ

17

426   167.0, 166.7, 153.9, 134.9, 133.6, 132.3, 131.7, 130.4, 128, 127.3, 126.3, 123.5, 122.9;

427   MS(ESI) $C_{14}H_9NO_2S$, $[M + H]^+$, m/z calcd 256.0426, found 256.0407.

428

429   **BT8** (methyl 4-(1,3-benzothiazol-2-yl)-benzoate): solid brown, 67 % yield. mp 158 ºC

430   ^{1}H NMR (400 MHz, DMSO-d_6) δ 8.25 (d, 2H, ^3J= 8.8 Hz), 8.21 (dd, 1H, J=1), 8.14 (d,

431   2H, ^3J= 8.8 Hz), 7.6 (td, 1H, ^3J= 7.6 Hz, ^4J= 1.2 Hz), 7.52 (td, 1H, ^3J= 7.7 Hz, ^4J= 1.2

432   Hz), 3.91 (s, 3H); ^{13}C NMR (101 MHz, DMSO-d_6) δ 166.4, 166.0, 153.9, 137.2, 135.2,

433   132.1, 130.6 (2C), 127.9 (2C), 127.4, 126.5, 123.7, 123.0, 52.8; MS(ESI) $C_{15}H_{11}NO_2S$,

434    $[M + H]^+$, m/z calcd 270.0583, found 270.0563.

435

436   **BT9** (methyl 3-(1,3-benzothiazol-2-yl)-benzoate): white powder, 87 % yield. mp 248

437   ºC. ^{1}H NMR (750 MHz, DMSO-d_6) δ 8.62 (s, 1H), 8.32 (d,1H ^3J= 8.25 Hz,), 8.17

438   (d,1H, ^3J= 7.5 Hz,), 8.11 (t, 2H, ^3J= 8.25 Hz), 7.73 (t, 1H, ^3J= 7.5 Hz,), 7.57 (t, 1H, ^3J=

439   7.87 Hz), 7.49 (t, 1H, ^3J= 7.87 Hz), 3.92 (s, 3H); ^{13}C NMR (189 MHz, DMSO-d_6) δ

440   166.5, 166, 153.9, 134.9, 133.7, 132.2, 132.0, 131.1, 130.6, 127.6, 127.3, 126.3, 123.5,

441   122.9, 52.9; MS(ESI) $C_{15}H_{11}NO_2S$, $[M + H]^+$, m/z calcd 270.0583, found 270.0575.

442

443   **BT10**   (2-methoxy-4-[5-(trifluoromethyl)-1,3-benzothiazol-2-yl]phenol):   Brownish

444   crystalline powder, 22 % yield. mp 137 ºC. ^{1}H NMR (300 MHz, DMSO-d_6) 8.3 (d, 1H,

445   ^3J= 6 Hz), 8.28 (s, 1H), 7.68 (dd, 1H, ^3J= 9 Hz, ^4J= 3 Hz), 7.6 (d, 1H, ^3J= 3 Hz), 7.51

446   (dd, 1H, ^3J= 8.4 Hz, ^4J= 2.1 Hz), 6.94 (d, 1H, ^3J= 8.1 Hz), 3.87 (s, 3H); ^{13}C NMR (75

447   MHz, DMSO- d_6) δ 170.6, 153.7, 151.0, 148.5, 138.8, 128, 124.1, 123.9, 122.1, 121.3,

448   119.3, 116.4, 110.6, 56.1; MS(ESI) $C_{15}H_{10}F_3NO_2S$, $[M + H]^+$, m/z calcd 326.0457,

449   found 326.0429.

450

451 **BT11** (4-(1,3-benzothiazol-2-yl)-2,6-dimethoxyphenol): grey crystals, 85 % yield. mp

452 135 ºC ^{1}H NMR (750 MHz, CDCl$_3$) δ 8.03 (d, 1H, ^3J= 8.25 Hz), 7.87 (d, 1H, ^3J= 7.5

453 Hz), 7.47 (m, 1H), 7.35 (td, 1H, ^3J= 7.5 Hz), 7.34 (s, 2H), 3.99 (s, 6H); ^{13}C NMR (189

454 MHz, CDCl$_3$) δ 168.1, 154.0, 147.3 (2C), 137.7, 134.8, 126.3, 125.1, 124.9, 122.8,

455 121.5, 104.5 (2C), 56.5 (2C); MS(ESI) C$_{15}$H$_{13}$NO$_3$S, [M + H]$^+$, m/z calcd 288.0689,

456 found 288.0695.

457

458 **BT12** (4-(1,3-benzothiazol-2-yl)benzonitrile): white crystalline powder, 88 % yield. mp

459 158 ºC. ^{1}H NMR (300 MHz, DMSO-d$_6$) δ 8.21 (d, 2H, J = 8.4 Hz), 8.16 (d, 1H, J = 8.1

460 Hz), 8.08 (d, 1H, J = 8.07 Hz), 7.98 (d, 2H, J = 8.4 Hz), 7.56 (m, 1H), 7.49 (t, 1H, J=

461 7.5 Hz); ^{13}C NMR (75 MHz, DMSO-d$_6$) δ 165.7, 153.8, 137.0, 135.3, 133.7 (2C), 128.2

462 (2C), 127.4, 126.6, 123.8, 123.0, 118.7, 113.7; MS(ESI) C$_{14}$H$_8$N$_2$S, [M + H]$^+$, m/z calcd

463 237.0481, found 237.0482.

464

465 **BT13** (2-(4-chlorophenyl)-1,3-benzothiazole): grey crystals, 72 % yield. mp 105 ºC. ^{1}H

466 NMR (750 MHz, CDCl$_3$) δ 8.06 (d, 1H, ^3J= 8.2 Hz), 8.02 (d, 2H, ^{3}J= 9 Hz, ^{4}J= 2.25

467 Hz), 7.9 (d, 1H, ^{3}J= 8.2 Hz), 7.5 (t, 1H, ^{3}J= 7.5 Hz), 7.46 (d, 2H, ^{3}J= 9 Hz, ^{4}J= 2.25 Hz),

468 7.39 (td, 1H, J= 7.12 Hz); ^{13}C NMR (189 MHz, CDCl$_3$) δ 166.6, 154.0, 137.0, 135.0,

469 132.1, 129.2 (2C), 128.7 (2C), 126.4, 125.4, 123.2, 121.6; MS(ESI) C$_{13}$H$_8$NSCl, [M +

470 H]$^+$, m/z calcd 246.0139, found 246.0134.

471

472 **BT14** (2-(4-bromophenyl)-1,3-benzothiazole): yellow crystals, 38 % yield. mp 124 ºC.

473 ^{1}H NMR (750 MHz, CDCl$_3$) δ 8.06 (d, 1H, ^3J = 8.2 Hz), 7.95 (d, 2H, ^3J= 8 Hz), 7.89 (d,

474 1H, ^3J= 8.2 Hz), 7.62 (d, 2H, ^{3}J= 8.2 Hz), 7.49 (t, 1H, ^{3}J= 7.5 Hz), 7.39 (td, 1H, ^3J= 7.5

475 Hz); ^{13}C NMR (189 MHz, CDCl$_3$) δ 166.6, 154.0, 135.0, 132.5, 132.2 (2C), 128.9 (2C),

476   126.5, 125.4, 123.3, 121.6; MS(ESI) $C_{13}H_8NSBr$, $[M + H]^+$, m/z calcd 289.9634, found

477   289.9613.

478

479

480   **Cells and parasite cultures.** *T. cruzi* epimastigotes (CL strain clone 14) were

481   maintained in the exponential growth phase by subculturing every 48 h in LIT medium

482   at 28 °C (44). The Chinese Hamster Ovary cell line (CHO-K_1) was cultivated in RPMI-

483   1640 medium supplemented with 10% heat-inactivated FCS, 0.15% (w/v) $NaHCO_3$,

484   100 units/mL penicillin and 100 mg/mL streptomycin at 37 °C in a humidified

485   atmosphere containing 5% CO_2. Trypomastigotes were obtained by infection in CHO-

486   K_1 cells with trypomastigotes at 37 °C in the presence of 10% FCS. After 24 h, the cells

487   were maintained at 33 °C and 2% FCS (45). Trypomastigotes were collected from the

488   extracellular medium five days after infection.

489

490   *In vitro* **inhibition of proliferation assays.** The cell density of exponentially

491   proliferating epimastigotes (approximately 50×10^6 parasites/mL) was adjusted to

492   2.5×10^6 cells/mL and transferred (200 μL/well) into 96-well plates (46). Epimastigote

493   proliferation was measured by reading the optical density (OD) at 620 nm every 24 h

494   through the exponential and stationary phases (9 days). The OD values were converted

495   to cell density values (cells per millilitre by using a calibration curve obtained by

496   measuring the OD values at 620 nm of parasite suspensions at different known

497   densities. The concentrations of the compound that inhibited 50% of epimastigote

498   proliferation (IC_{50}) were determined in the exponential growth phase (5th day) by fitting

499   the cell density data to a sigmoidal concentration-response curve using GraphPad Prism

500   v.6. A combination of 60 μM rotenone and 0.5 μM antimycin A (RA) was used as a

20

501   positive control for proliferation inhibition. Untreated parasites supplemented with

502   DMSO (the vehicle for the drugs) and unsupplemented parasites were used as negative

503   controls. The compounds were evaluated in quadruplicate in each experiment, and the

504   results correspond to three independent experiments.

505

506   **The effect of BT3 and BT10 compounds on mammalian cell viability.** CHO-K_1 cells

507   (1×10^5 cells/well) in 100 μL of RPMI medium supplemented with FCS (10%) were

508   seeded in 96-well plates with or without (control) different concentrations of the most

509   active compounds, BT3 (16 to 800 μM) and BT10 (8 to 288 μM). Cell viability was

510   determined by the MTT assay as previously described (47). The produced formazan was

511   solubilized in 50 μL of DMSO, and the optical density (OD) was measured at 540 nm

512   using 690 nm as a reference. The IC_{50} was determined by fitting the data to a sigmoidal

513   dose-response curve using GraphPad Prism v.6. Each assay was developed in

514   quadruplicate, and the results correspond to the mean of three independent experiments.

515

516   **Analysis of phosphatidylserine exposure, mitochondrial inner membrane ($\Delta\Psi_m$)**

517   **depolarization, intracellular Ca^{2+} levels, and hydrogen peroxide production.**

518   Epimastigotes (2.5×10^6 cell/mL) were incubated for five days, unless otherwise stated,

519   in the presence or absence (control) of 25 μM and 50 μM BT10 (approximately 1x and

520   2x the IC_{50}, respectively). To determine phosphatidylserine exposure, the cells were

521   labelled with propidium iodide (PI) and Annexin-V FITC (Molecular Probes) according

522   to the manufacturer's instructions. As positive controls for cytoplasmic membrane

523   permeabilisation and extracellular exposure of phosphatidylserine, the parasites were

524   treated with 150 μM digitonin or 1μM staurosporine for 30 min, respectively (48). For

525   determining variations in $\Delta\Psi_m$, cells were aliquoted in fractions at densities of 1.0×10^6

21

526   cells/mL. One half of the aliquot was incubated for 15 min with 1 μM FCCP in PBS,

527   while the other half was left untreated. Then, all samples were centrifuged for 10 min at

528   2,700 x g and resuspended in HEPES-glucose buffer (50 mM HEPES (pH 7.4), 116 mM

529   NaCl, 5.4 mM KCl, 0.8 mM $MgSO_4$, 5.5 mM glucose, and 2 mM $CaCl_2$). The cells

530   were labelled by the addition of 256 nM Rhodamine 123 (Rh123) for 20 min at 28 °C

531   (49). To analyse variations in the intracellular Ca^{2+} levels, the parasites were incubated

532   with 5 mM Fluo-4 AM (Invitrogen) for one hour at 28 °C. After this period, the cells

533   were washed twice with HEPES-glucose and resuspended in the same buffer (50). To

534   evaluate the production of hydrogen peroxide, the parasites treated with $1xIC_{50}$ or

535   $2xIC_{50}$ of BT10 during 24 h were incubated for 30 min at 28 °C in HEPES-glucose

536   buffer in the presence of 10 μM of carboxy-DCFDA. In all cases, the cells were

537   analysed by flow cytometry on a Guava cytometer (General Electric), with 10,000

538   events collected, and analysed using FlowJo software (v10.1r7).

539

540   **DNA content and cell cycle analysis.** Parasites (2.5×10^6 cells/mL) treated with 25 and

541   100 μM BT10 (or not, negative control) for five days were collected by centrifugation

542   (2,700 x g for 5 min), washed in PBS, fixed in 70% ethanol for 12 h, and incubated with

543   10 μg/mL RNase A (Thermo Scientific) for 30 min at 37 °C. To measure the DNA

544   content, parasite cells were stained with 40 μg/mL propidium iodide (Molecular

545   Probes/Invitrogen) and analysed by flow cytometry on an acoustic focusing cytometer

546   (Attune; Applied Biosystems), with 50,000 events collected (31). Histograms (number

547   of counts by BL2 area) scatter plots (side scatter [SSC] area by forward scatter [FSC]

548   area) and gates for each cell cycle phase were analysed using FlowJo software

549   (v10.1r7). Cell cycle data were fitted using Dean-Jett Fox (DJF) model included in the

550   FlowJo software.

22

551

Analysis of DNA damage by TUNEL assay. Epimastigotes treated with 25 μM BT10

(or not, control) in the exponential growth phase were collected by centrifugation,

washed with PBS and fixed by incubation with 4% paraformaldehyde for 10 min at

room temperature. After washing and resuspension in PBS, the cells were permeabilized

by treatment with 0.1% Triton X-100 for 10 min at 26 ºC and were treated with 0.1 M

glycine for 5 min to neutralize the remaining aldehyde groups. The TUNEL assay was

performed by using the DeadEnd™ Fluorometric TUNEL System Promega kit (G3250)

according to the manufacturer's protocol. VECTASHIELD® Mounting Medium with

DAPI (Vector Labs) was added to be used as an anti-fade mounting solution and to stain

nuclear and kinetoplast DNA. For each group analysed, we analysed at least 100 cells in

at least three different image fields. This assay was carried out in triplicate. To confirm

these results, we analysed an aliquot of the cells in each condition by cytometry.

Histograms (counts x BL1 area), scatter plots (SSC-area x FSC-area) and gates to

exclude cell debris/doublets were performed using Attune Cytometric Software (v.1.2.5)

and FlowJo software (v10.1r7). In total, 10,000 events were analysed for each sample.

567

Effect of BT10 on amastigote replication and trypomastigote release. CHO-K_1 cells

$(5.0 \times 10^4$ per well) were maintained in 24-well plates in RPMI medium supplemented

with 10% FCS at 37 °C. To perform the infections, the cells were incubated with

trypomastigote forms $(2.5 \times 10^6$ per well) for 4 h. After this period, parasites in the

supernatant were removed by washing the plates twice with PBS, and the cells were

incubated overnight in RPMI medium supplemented with 10% FCS at 37 °C in the

presence of different concentrations of BT10 or left untreated (control). The plates were

then incubated at 33 °C to allow the parasite to complete the infection cycle, as

23

576   previously reported (46). To measure the effect on amastigote replication, after 48 h, the

577   CHO-K$_1$ cells and parasites were fixed with 4% paraformaldehyde, and nuclei were

578   stained with Hoechst 33342 (Invitrogen) for counting. We acquired fluorescence

579   microscopy images corresponding to 30 fields per biological sample at a magnification

580   of 200x (EVOS FL Cell Imaging System, Thermo Fisher Scientific). Cells, parasites,

581   and infected cells were counted using ImageJ software. The infection index was

582   calculated as the arithmetical product of the percentage of infected cells and the number

583   of parasites per cell. The effect of BT10 on trypomastigote production was determined

584   by collecting samples of the extracellular medium on the fifth day post-infection and

585   counting the number of trypomastigotes in a Neubauer chamber (40). The results

586   correspond to the mean of three independent experiments, each performed in triplicate.

587

588   **Data treatment and statistical analysis.** Curve adjustments, regressions, and statistical

589   analyses were performed with the GraphPad Prism 7 analysis tools. All assays were

590   performed at least in biological triplicates. The specific details of the statistical analysis

591   for each experiment are described in the corresponding figure legend. In general, The

592   Student's *t*-test was used to analyse differences between the two groups. P values of less

593   than 0.05 were considered statistically significant.

594

595   **Author contributions**

596   Synthesised and characterized compounds: RICH, JGTF, SMC. Conceived and

597   designed the biological experiments: RG, RICH, AMS. Performed the experiments:

598   RICH, RG, MC, AMS, MSS. Analysed the data: RICH, RG, AMS, MCE. Contributed

599   reagents/materials/analysis tools: JGTF, AMS. Wrote the paper: RICH, AMS, RG. All

600   authors have given approval to the final version of the paper.

24

601

602

616

617 **References**

618 1.   2018. WHO | Chagas disease (American trypanosomiasis). WHO. World Health

619   Organization.

620 2.   **Bonney KM.** 2014. Chagas disease in the 21st century: a public health success or an

621   emerging threat? Parasite **21**:11.

622 3.   **Bern C.** 2015. Chagas' Disease. N Engl J Med **373**:456–466.

623 4.   **Liu Q, Zhou X-N.** 2015. Preventing the transmission of American trypanosomiasis and

624   its spread into non-endemic countries. Infect Dis poverty **4**:60.

625 5.   **Brener Z.** 1973. Biology of *Trypanosoma Cruzi*. Annu Rev Microbiol **27**:347–382.

626 6.   **Alves MJM, Colli W.** 2007. *Trypanosoma cruzi*: Adhesion to the Host Cell and

25

627   Intracellular Survival. IUBMB Life **59**:274–279.

628   7.   **Purser S, Moore PR, Swallow S, Gouverneur V.** 2008. Fluorine in medicinal chemistry.

629   Chem Soc Rev **37**:320–30.

630   8.   **Boscardin SB, Torrecilhas ACT, Manarin R, Revelli S, Rey EG, Tonelli RR, Silber AM.**

631   2010. Chagas' disease: an update on immune mechanisms and therapeutic strategies. J

632   Cell Mol Med **14**:1373–1384.

633   9.   **Rassi A, Rassi A, Marin-Neto JA.** 2010. Chagas disease. Lancet (London, England)

634   **375**:1388–402.

635   10.   **Gouttefangeas C, Britten CM, Badalians ED, Pawelec G.** 2006. CIMT meets Strategies

636   for Immune Therapy: Mainz, Germany, 04–05 May 2006. Cancer Immunol Immunother

637   **56**:397–402.

638   11.   **Jensen RE, Englund PT.** 2012. Network News: The Replication of Kinetoplast DNA. Annu

639   Rev Microbiol **66**:473–491.

640   12.   **Duschak VG.** 2016. Targets and Patented Drugs for Chemotherapy of Chagas Disease in

641   the Last 15 Years-Period. Recent Pat Antiinfect Drug Discov **11**:74–173.

642   13.   **Téllez-Valencia A, Ávila-Ríos S, Pérez-Montfort R, Rodríguez-Romero A, Tuena de**

643   **Gómez-Puyou M, López-Calahorra F, Gómez-Puyou A.** 2002. Highly specific inactivation

644   of triosephosphate isomerase from *Trypanosoma cruzi*. Biochem Biophys Res Commun

645   **295**:958–963.

646   14.   **Cuevas-Hernández RI, Correa-Basurto J, Flores-Sandoval CA, Padilla-Martínez II,**

647   **Nogueda-Torres B, Villa-Tanaca MDL, Tamay-Cach F, Nolasco-Fidencio JJ, Trujillo-**

648   **Ferrara JG.** 2016. Fluorine-containing benzothiazole as a novel trypanocidal agent:

649   design, in silico study, synthesis and activity evaluation. Med Chem Res **25**:211–224.

650   15.   **Patrick DA, Gillespie JR, McQueen J, Hulverson MA, Ranade RM, Creason SA, Herbst**

651   **ZM, Gelb MH, Buckner FS, Tidwell RR.** 2017. Urea Derivatives of 2-Aryl-benzothiazol-5-

652   amines: A New Class of Potential Drugs for Human African Trypanosomiasis. J Med

653   Chem **60**:957–971.

654   16.   **Bae H-J, Lee Y-S, Kang D-W, Gu J-S, Yoon B-W, Roh J-K.** 2000. Neuroprotective effect of

655   low dose riluzole in gerbil model of transient global ischemia. Neurosci Lett **294**:29–32.

656   17.   **Kumar P, Shrivastava B, Pandeya SN, Tripathi L, Stables JP.** 2012. Design, synthesis,

657   and anticonvulsant evaluation of some novel 1, 3 benzothiazol-2-yl

658   hydrazones/acetohydrazones. Med Chem Res **21**:2428–2442.

659   18.   **Cressier D, Prouillac C, Hernandez P, Amourette C, Diserbo M, Lion C, Rima G.** 2009.

660   Synthesis, antioxidant properties and radioprotective effects of new benzothiazoles and

661   thiadiazoles. Bioorg Med Chem **17**:5275–5284.

662   19.   **Ha YM, Park JY, Park YJ, Park D, Choi YJ, Kim JM, Lee EK, Han YK, Kim J-A, Lee JY,**

663   **Moon HR, Chung HY.** 2011. Synthesis and biological activity of hydroxy substituted

664   phenyl-benzo[d]thiazole analogues for antityrosinase activity in B16 cells. Bioorg Med

665   Chem Lett **21**:2445–2449.

666   20.   **Mortimer CG, Wells G, Crochard J-P, Stone EL, Bradshaw TD, Stevens MFG, Westwell**

667   **AD.** 2006. Antitumor Benzothiazoles. 26. 1 2-(3,4-Dimethoxyphenyl)-5-

668   fluorobenzothiazole (GW 610, NSC 721648), a Simple Fluorinated 2-Arylbenzothiazole,

669   Shows Potent and Selective Inhibitory Activity against Lung, Colon, and Breast Cancer

670   Cell Lines. J Med Chem **49**:179–185.

671   21.   **Hiyoshi H, Goto N, Tsuchiya M, Iida K, Nakajima Y, Hirata N, Kanda Y, Nagasawa K,**

672   **Yanagisawa J.** 2015. 2-(4-Hydroxy-3-methoxyphenyl)-benzothiazole suppresses tumor

673   progression and metastatic potential of breast cancer cells by inducing ubiquitin ligase

674   CHIP. Sci Rep **4**:7095.

675   22.   **Sahu PK, Sahu PK, Gupta SK, Thavaselvam D, Agarwal DD.** 2012. Synthesis and

676   evaluation of antimicrobial activity of 4H-pyrimido[2,1-b]benzothiazole, pyrazole and

677   benzylidene derivatives of curcumin. Eur J Med Chem **54**:366–78.

678   23.   **Delmas F, Avellaneda A, Di Giorgio C, Robin M, De Clercq E, Timon-David P, Galy J-P.**

679   2004. Synthesis and antileishmanial activity of (1,3-benzothiazol-2-yl) amino-9-(10H)-

680   acridinone derivatives. Eur J Med Chem **39**:685–690.

681 24. **Espinoza-Fonseca LM, Trujillo-Ferrara JG.** 2006. Toward a rational design of selective

682   multi-trypanosomatid inhibitors: A computational docking study. Bioorg Med Chem Lett

683   **16**:6288–6292.

684 25. **Olivares-Illana V, Pérez-Montfort R, López-Calahorra F, Costas M, Rodríguez-Romero**

685   **A, Tuena de Gómez-Puyou M, Gómez Puyou A.** 2006. Structural differences in

686   triosephosphate   isomerase   from   different   species   and   discovery   of   a

687   multitrypanosomatid inhibitor. Biochemistry **45**:2556–60.

688 26. **Smirlis D, Duszenko M, Ruiz A, Scoulica E, Bastien P, Fasel N, Soteriadou K.** 2010.

689   Targeting   essential   pathways   in   trypanosomatids   gives   insights   into   protozoan

690   mechanisms of cell death. Parasit Vectors **3**:107.

691 27. **Smirlis D, Soteriadou K.** 2011. Trypanosomatid apoptosis: "Apoptosis" without the

692   canonical regulators. Virulence **2**:253–256.

693 28. **Irigoín F, Inada NM, Fernandes MP, Piacenza L, Gadelha FR, Vercesi AE, Radi R.** 2009.

694   Mitochondrial calcium overload triggers complement-dependent superoxide-mediated

695   programmed cell death in Trypanosoma cruzi. Biochem J **418**:595–604.

696 29. **Selvarajah J, Elia A, Carroll VA, Moumen A.** 2015. DNA damage-induced S and G2/M

697   cell cycle arrest requires mTORC2-dependent regulation of Chk1. Oncotarget **6**:427–40.

698 30. **Yin M, Guo B, Panadero A, Frank C, Wrzosek C, Slocum HK, Rustum YM.** 1999. Cyclin

699   E–Cdk2 Activation Is Associated with Cell Cycle Arrest and Inhibition of DNA Replication

700   Induced by the Thymidylate Synthase Inhibitor Tomudex. Exp Cell Res **247**:189–199.

701 31. **Zuma AA, Mendes IC, Reignault LC, Elias MC, de Souza W, Machado CR, Motta MCM.**

702   2014. How *Trypanosoma cruzi* handles cell cycle arrest promoted by camptothecin, a

703   topoisomerase I inhibitor. Mol Biochem Parasitol **193**:93–100.

704 32. **Smart BE.** 2001. Fluorine substituent effects (on bioactivity). J Fluor Chem **109**:3–11.
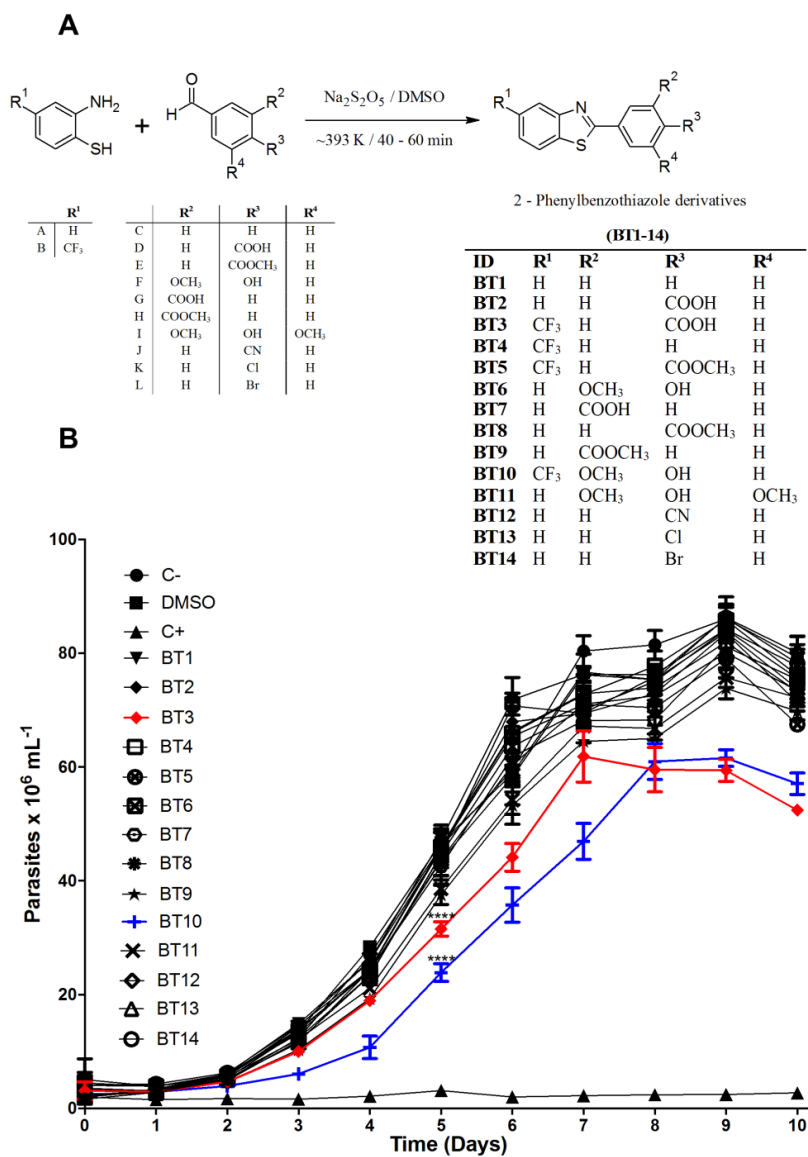
705   33.   **Purser S, Moore PR, Swallow S, Gouverneur V.** 2008. Fluorine in medicinal chemistry.

706   Chem Soc Rev **37**:320–330.

707   34.   **Swallow S.** 2015. Fluorine in Medicinal Chemistry, p. 65–133. In Progress in Medicinal

708   Chemistry, 1st ed. Elsevier B.V.

709   35.   **Lipinski CA, Lombardo F, Dominy BW, Feeney PJ.** 2001. Experimental and

710   computational approaches to estimate solubility and permeability in drug discovery and

711   development settings. Adv Drug Deliv Rev **46**:3–26.

712   36.   **Ertl P, Rohde B, Selzer P.** 2000. Fast calculation of molecular polar surface area as a

713   sum of fragment-based contributions and its application to the prediction of drug

714   transport properties. J Med Chem.

715   37.   **Xuejiao S, Yong X, Ningyu W, Lidan Z, Xuanhong S, Youzhi X, Tinghong Y, Yaojie S,**

716   **Yongxia Z, Luoting Y.** 2013. A Novel Benzothiazole Derivative YLT322 Induces Apoptosis

717   via the Mitochondrial Apoptosis Pathway *In Vitro* with Anti-Tumor Activity in Solid

718   Malignancies. PLoS One **8**:e63900.

719   38.   **Wang Z, Shi X-H, Wang J, Zhou T, Xu Y-Z, Huang T-T, Li Y-F, Zhao Y-L, Yang L, Yang S-Y,**

720   **Yu L-T, Wei Y-Q.** 2011. Synthesis, structure–activity relationships and preliminary

721   antitumor evaluation of benzothiazole-2-thiol derivatives as novel apoptosis inducers.

722   Bioorg Med Chem Lett **21**:1097–1101.

723   39.   **Selvarajah J, Elia A, Carroll VA, Moumen A.** 2015. DNA damage-induced S and G2/M

724   cell cycle arrest requires mTORC2-dependent regulation of Chk1. Oncotarget **6**:427–40.

725   40.   **Girard RMBM, Crispim M, Stolić I, Damasceno FS, Santos da Silva M, Pral EMF, Elias**

726   **MC, Bajić M, Silber AM.** 2016. An Aromatic Diamidine That Targets Kinetoplast DNA,

727   Impairs the Cell Cycle in *Trypanosoma cruzi*, and Diminishes Trypomastigote Release

728   from Infected Mammalian Host Cells. Antimicrob Agents Chemother **60**:5867–5877.

729   41.   **Cuevas-Hernández R, Padilla-Martínez I, Martínez-Cerón S, Vásquez-Moctezuma I,**

730   **Trujillo-Ferrara J.** 2017. Helical Arrangement of 2-(4-hydroxy-3-methoxyphenyl)-

29

731   Benzothiazole in Crystal Formation and Biological Evaluation on HeLa Cells. Crystals

732   **7**:171.

733 42. **Espinoza-Fonseca LM, Trujillo-Ferrara JG.** 2006. Toward a rational design of selective

734   multi-trypanosomatid inhibitors: A computational docking study. Bioorg Med Chem Lett

735   **16**:6288–6292.

736 43. **DON R, IOSET J-R.** 2014. Screening strategies to identify new chemical diversity for drug

737   development to treat kinetoplastid infections. Parasitology **141**:140–146.

738 44. **Brener Z, Chiari E.** 1965. Aspects of early growth of different *Trypanosoma cruzi* strains

739   in culture medium. J Parasitol **51**:922–6.

740 45. **Almeida-de-Faria M, Freymüller E, Colli W, Alves MJM.** 1999. *Trypanosoma cruzi*:

741   Characterization of an intracellular epimastigote- like form. Exp Parasitol **92**:163–274.

742 46. **Magdaleno A, Ahn I-Y, Paes LS, Silber AM.** 2009. Actions of a Proline Analogue, L-

743   Thiazolidine-4-Carboxylic Acid (T4C), on *Trypanosoma cruzi*. PLoS One **4**:e4534.

744 47. **Mosmann T.** 1983. Rapid colorimetric assay for cellular growth and survival: application

745   to proliferation and cytotoxicity assays. J Immunol Methods **65**:55–63.

746 48. **Jimenez V, Paredes R, Sosa MA, Galanti N.** 2008. Natural programmed cell death in *T.

747   cruzi* epimastigotes maintained in axenic cultures. J Cell Biochem **105**:688–698.

748 49. **Girard RMBM, Crispim M, Alencar MB, Silber AM.** 2018. Uptake of l-Alanine and Its

749   Distinct Roles in the Bioenergetics of *Trypanosoma cruzi*. mSphere **3**:e00338-18.

750 50. **Dolai S, Yadav RK, Pal S, Adak S.** 2009. Overexpression of Mitochondrial *Leishmania

751   major* Ascorbate Peroxidase Enhances Tolerance to Oxidative Stress-Induced

752   Programmed Cell Death and Protein Damage. Eukaryot Cell **8**:1721–1731.

753

754   **Figures and legends**

755

A

2 - Phenylbenzothiazole derivatives

	R^1
A	H
B	CF_3

	R^2	R^3	R^4
C	H	H	H
D	H	COOH	H
E	H	$COOCH_3$	H
F	OCH_3	OH	H
G	COOH	H	H
H	$COOCH_3$	H	H
I	OCH_3	OH	OCH_3
J	H	CN	H
K	H	Cl	H
L	H	Br	H

(BT1-14)

| ID	R^1	R^2	R^3	R^4
BT1	H	H	H	H
BT2	H	H	COOH	H
BT3	CF_3	H	COOH	H
BT4	CF_3	H	H	H
BT5	CF_3	H	$COOCH_3$	H
BT6	H	OCH_3	OH	H
BT7	H	COOH	H	H
BT8	H	H	$COOCH_3$	H
BT9	H	$COOCH_3$	H	H
BT10	CF_3	OCH_3	OH	H
BT11	H	OCH_3	OH	OCH_3
BT12	H	H	CN	H
BT13	H	H	Cl	H
BT14	H	H	Br	H

B

756
757

758   **Figure 1. Synthesis of 2-phenylbenzothiazole derivatives and screening assay for**

759   **selection of the best active compounds on the proliferation growth curves of**

760   **epimastigote forms of _T. cruzi_. A)** Schematic synthesis strategy and structure of 2-

761   phenylbenzothiazole derivatives; **B)** Growth curves in the presence of 25 μM each

762   compound proposed. A combination of 60 μM rotenone + 0.5 μM antimycin was used

763   as a positive control (C+). The figure shows a representative proliferation curve of three

764   independent experiments. The values are plotted as the mean ± SD and compared on the

765   5th day of proliferation to the control (C-) using a *t*-test. ****, P < 0.0001 to establish

766   significant differences.

767
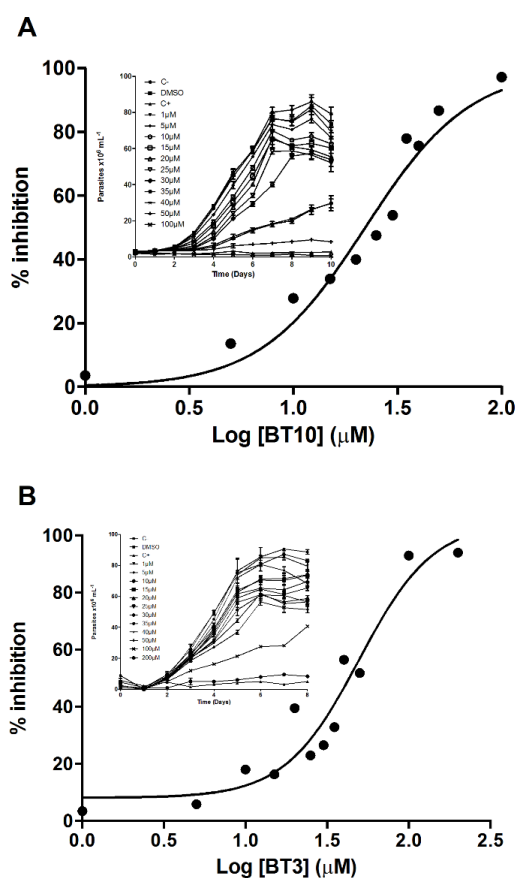
768

769   **Figure 2. Effects of BT3 and BT10 on the proliferation of the epimastigote form of**

770   ***Trypanosoma cruzi.* A)** Growth inhibition curves in the presence of different

771   concentrations of BT10 at 28ºC, which is the optimum temperature of proliferation, IC_{50}

772   = 23.1 ± 1.75 μM. **B)** Growth inhibition curves in the presence of different

773   concentrations of BT3 at 28ºC, IC_{50} = 48.8 ± 5.77 μM. A combination of 60 μM

32

774   rotenone + 0.5 μM antimycin was used as a positive control (C+). The IC_{50} values were

775   obtained by adjusting the data to nonlinear regression. Figures show a representative

776   proliferation curve of three independent experiments for each condition.

777
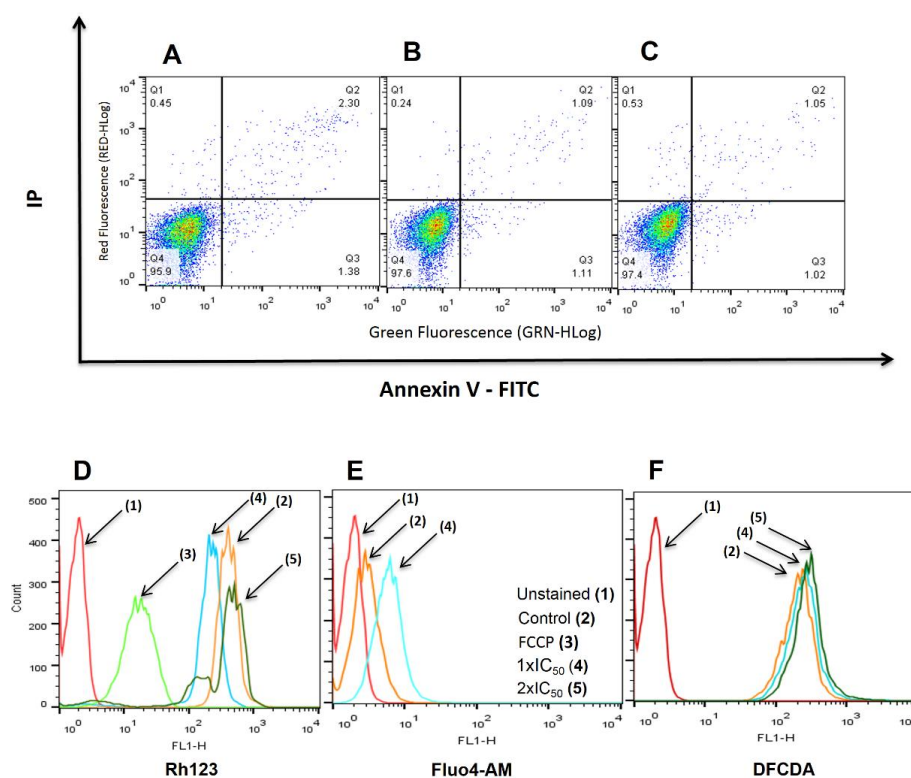
778

779   **Figure 3. Analysis of cell death type and viability in epimastigotes treated with**

780   **BT10. Analysis of extracellular exposure of phosphatidylserine by annexin**

781   **V/propidium iodide labelling by flow cytometry on epimastigotes treated with**

782   **BT10 during five days**: **(A)** Non-treated parasites, **B)** parasites treated with $1xIC_{50}$ (25

783   μM) BT10 and **C)** parasites treated with $2xIC_{50}$ (50 μM) BT10. **Analysis of cell**

784   **viability of epimastigotes treated with BT10 during five days**: **D)** membrane

785   depolarization test (ΔΨm), **E)** quantification of intracellular Ca^{2+} and **F)** analysis of the

786   generation of ROS after 24 h of treatment with BT10. Figures are representative of three

787   independent experiments. The values were plotted as the mean ± SEM and compared to

788   the control using a *t*-test. *, P < 0.05 to establish significant differences.

789
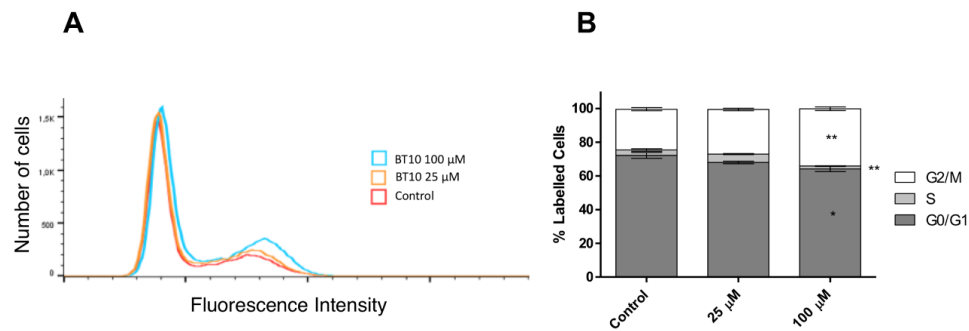
790

791   **Figure 4**. **Effect of BT10 on the epimastigote cell cycle using FACS**. Cells were

792   treated or not (control) with 25 µM or 100 µM BT10 for five days in the exponential

793   growth. After that time, parasites were washed, treated with RNase A, and stained with

794   propidium iodide, and their DNA content was analysed by fluorescence-activated cell

795   sorting. In total, 50,000 events were analysed for each sample. Histograms are shown in

796   **A,** and quantification of the percentage number of cells labelled in each stage of the cell

797   cycle is presented in **B**. The figure shows representative histograms of three

798   independent experiments. The values are plotted as the mean ± SEM and compared to

799   the control using a *t*-test. *, P < 0.05; ** P < 0.01 to establish significant differences.

800   The data correspond to three independent biological experiments.

801

34

802
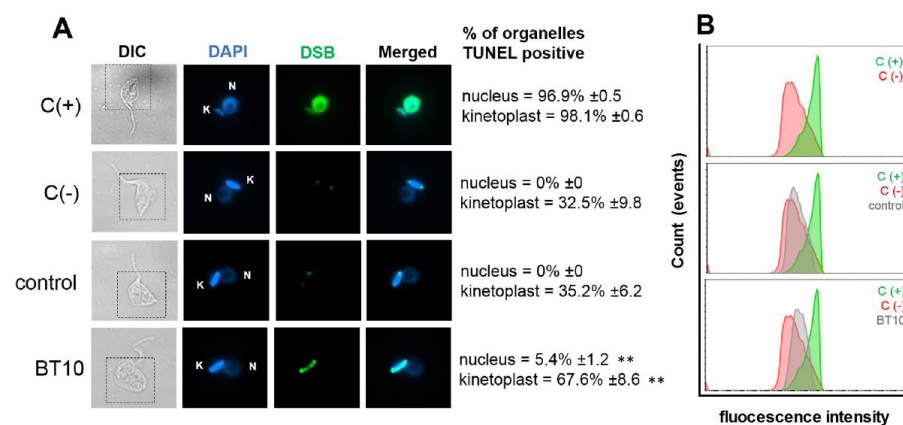
Figure 5. BT10 induces increased kDNA fragmentation. **A**. Control and cells treated with 25 μM BT10 for five days were submitted to TUNEL assay to indicate DNA strand breaks – DSBs (green). DAPI (blue) was used to show organelles that contain DNA (N = nucleus, k = kinetoplast). DIC and merged columns indicate the morphology of the cells and overlay between the DAPI and DSB columns, respectively. DNase I was used as a positive control, and the absence of TdT enzyme was used as a negative control. The percentage of TUNEL-positive organelles is displayed on the right of the panel. Images represent the pattern prevalent in each analysis. **B**. The same groups were analysed through the flow cytometry, and the histograms (counts x fluorescence intensity – BL1-area) were plotted to show differences in fluorescence intensity between each group (treated and non-treated) and controls (positive and negative). In total, 10,000 events were analysed for each sample. The histograms shown are representative of three independent experiments. The increase in fluorescence intensity shown in the flow cytometer graphs and the percentage of TUNEL-positive organelles indicates that the BT10 compound is highly effective at generating an increased amount of DSBs within a single cell and in a larger number of cells. The values are plotted as the mean ± SEM and compared to the control using a *t*-test. ** $P < 0.01$ to establish

35

820   significant differences. The data correspond to three independent biological

821   experiments.

822
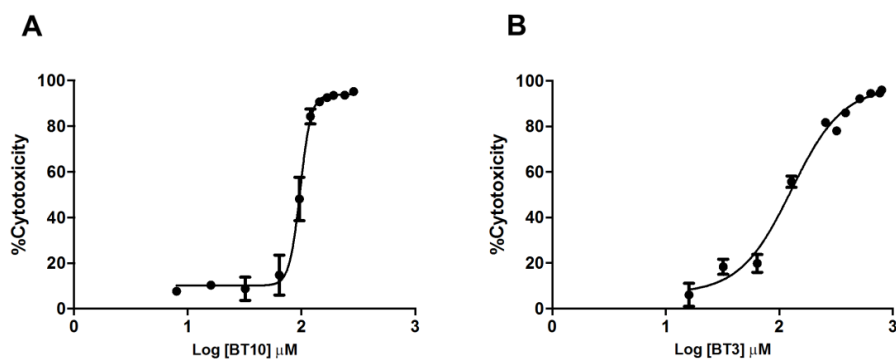
823

824

825   **Figure 6. Effect of BT10 and BT3 on mammalian cells.** The cell viability of CHO-K_1

826   cells treated with different concentrations of BT10 or BT3 for 48 h was assessed by

827   MTT assay, and the corresponding concentration-response curve of cytotoxicity was

828   expressed as a percentage of inhibition of proliferation. **A)** Dose response for cell

829   viability in the presence of different concentrations of BT10 (range: 8 to 288 μM), CC_{50}

830   = 95.3 ± 3.3 μM. **B)** Dose-response for cell viability in the presence of different

831   concentrations of BT3 (range: 16 to 800 μM), CC_{50} = 127.6 ± 0.9 μM. Figures show a

832   representative curve of three independent experiments.

833

36

834
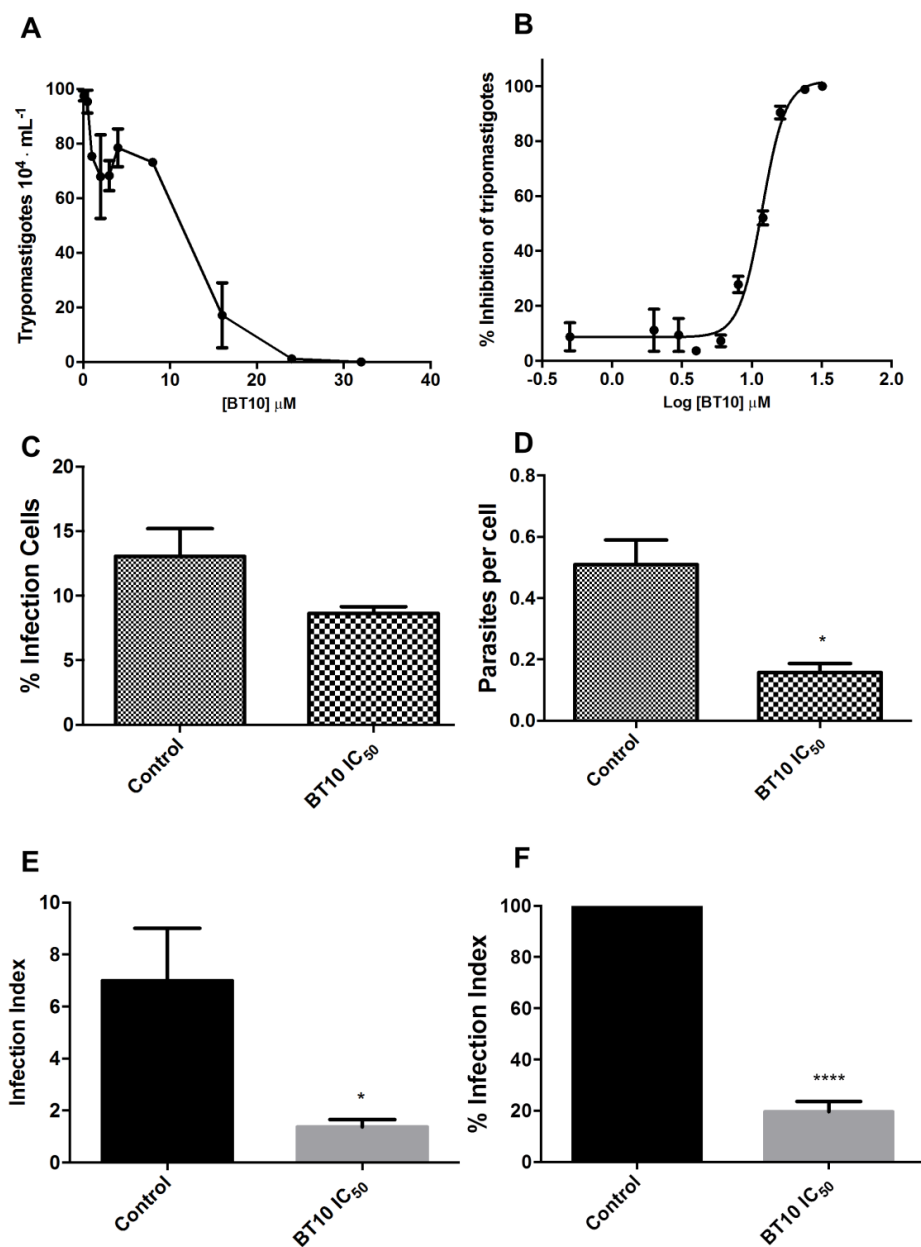
Figure 7. Effect of BT10 on intracellular cycle and amastigotes replication of *T. cruzi*. The effect of BT10 after infection on CHO-k$_1$ cells with trypomastigotes forms was evaluated by counting the released parasites in a Neubauer chamber at the fifth day post-infection **A)** and the corresponding concentration-response curve was plotted, IC$_{50(Tryp)}$ = 8.5 ± 2.9 μM **B)**. The percentage of the number of infected cells **C)** and the

840   number of intracellular amastigotes per cell **D)** were counted as described in material

841   and methods. The effect on amastigote replication was measured using the infection

842   index (% of infected cells x parasites per cells) of treated parasites with IC_{50} compared

843   to control **E)** and the percentage of the infected index of treated parasites with IC_{50}

844   compared to control **F)**. The values were plotted as the mean ± SEM and compared to

845   the control using a *t*-test. *, P < 0.05; **** P < 0.0001 to establish significant

846   differences. Figures A and B show a representative curve of three independent

847   experiments. Figures C, D, E and F correspond to three independent biological

848   experiments.

849

850

Table 1. The activity of BT3 and BT10 on different aspects of *T. cruzi*
biology

	BT10	BT3
Epi IC_{50} (µM) 28 ºC	23.1 ± 1.75	48.8 ± 5.77
CC_{50} (µM)	95.3 ± 3.3	127.6 ± 0.9
Tryp IC_{50} (µM)	8.5 ± 2.9	ND[a]
Selectivity Index (*SI*)		
SI: $CC_{50}/IC_{50(Epi)\ 28\ ºC}$	4.13	2.61
SI: $CC_{50}/IC_{50(Tryp)}$	11.21	ND
% infection index inhibition	81.3	ND
Loss of cytoplasmic membrane integrity	NO	NO
Induces ROS	NO	ND
Alters intracellular Ca^{2+}	NO	ND
Affect parasite cell cycle	Yes	ND
The reversible effect in Epi	Yes	ND
kDNA damage	Yes	Yes
Affects amastigote replication	Yes	ND
Affects host cell infection	Yes	ND

38

[a]ND, not determined.

851

A

$$R^1\text{-benzene-}NH_2 \ + \ \text{aldehyde-}R^2,R^3,R^4 \ \xrightarrow[\sim 393 \text{ K} / 40 - 60 \text{ min}]{Na_2S_2O_5 \ / \ DMSO} \ \text{2 - Phenylbenzothiazole derivatives}$$

	R^1
A	H
B	CF_3

	R^2	R^3	R^4
C	H	H	H
D	H	COOH	H
E	H	COOCH$_3$	H
F	OCH$_3$	OH	H
G	COOH	H	H
H	COOCH$_3$	H	H
I	OCH$_3$	OH	OCH$_3$
J	H	CN	H
K	H	Cl	H
L	H	Br	H

(BT1-14)

ID	R^1	R^2	R^3	R^4
BT1	H	H	H	H
BT2	H	H	COOH	H
BT3	CF$_3$	H	COOH	H
BT4	CF$_3$	H	H	H
BT5	CF$_3$	H	COOCH$_3$	H
BT6	H	OCH$_3$	OH	H
BT7	H	COOH	H	H
BT8	H	H	COOCH$_3$	H
BT9	H	COOCH$_3$	H	H
BT10	CF$_3$	OCH$_3$	OH	H
BT11	H	OCH$_3$	OH	OCH$_3$
BT12	H	H	CN	H
BT13	H	H	Cl	H
BT14	H	H	Br	H

B

A

B

IP

A

Q1
0.45

Q2
2.30

Q4
95.9

Q3
1.38

Red Fluorescence (RED-HLog)

B

Q1
0.24

Q2
1.09

Q4
97.6

Q3
1.11

C

Q1
0.53

Q2
1.05

Q4
97.4

Q3
1.02

Green Fluorescence (GRN-HLog)

Annexin V - FITC

D

(1)
(4) (2)
(3)
(5)

Count

FL1-H

Rh123

E

(1)
(2)
(4)

FL1-H

Fluo4-AM

Unstained **(1)**
Control **(2)**
FCCP **(3)**
$1 \times IC_{50}$ **(4)**
$2 \times IC_{50}$ **(5)**

F

(1)
(5)
(4)
(2)

FL1-H

DFCDA

A

B

A

	DIC	DAPI	DSB	Merged	% of organelles TUNEL positive
C(+)		N K			nucleus = 96.9% ±0.5 kinetoplast = 98.1% ±0.6
C(-)		N K			nucleus = 0% ±0 kinetoplast = 32.5% ±9.8
control		K N			nucleus = 0% ±0 kinetoplast = 35.2% ±6.2
BT10		K N			nucleus = 5.4% ±1.2 ** kinetoplast = 67.6% ±8.6 **

B

C (+)
C (-)

C (+)
C (-)
control

C (+)
C (-)
BT10

Count (events)

fluocescence intensity